Journal of Hazardous Materials 203–204 (2012) 111–117

Contents lists available at SciVerse ScienceDirect

Journal of Hazardous Materials

journal homepage: www.elsevier.com/locate/jhazmat

Adsorption equilibrium and kinetics for SO_2, NO, CO_2 on zeolites FAU and LTA

Honghong Yi, Hua Deng, Xiaolong Tang*, Qiongfen Yu, Xuan Zhou, Haiyan Liu

Faculty of Environmental Science and Engineering, Kunming University of Science and Technology, Kunming 650093, China

ARTICLE INFO

Article history:
Received 6 August 2011
Received in revised form 9 November 2011
Accepted 26 November 2011
Available online 8 December 2011

Keywords:
Simultaneous desulfurization
denitrification
Carbon capture
Equilibrium
Kinetics
Zeolite

ABSTRACT

In order to develop a single-step process for removing SO_2, NO, CO_2 in flue gas simultaneously by co-adsorption method. Pure component adsorption equilibrium and kinetics of SO_2, NO, and CO_2 on zeolite NaY, NaX, CaA were obtained respectively. Equilibrium data were analyzed by equilibrium model and Henry's law constant. The results suggest that Adsorption affinity follows the trend $SO_2 > CO_2 > NO$ for the same adsorbent. Zeolite with stronger polar surface is a more promising adsorbent candidate. Kinetics behavior was investigated using the breakthrough curve method. The overall mass transfer coefficient and diffusivity factor were determined by a linear driving force model. The results are indicative of micropore diffusion controlling mechanism. NaY zeolite has the minimum resistance of mass transfer duo to the wide pore distribution and large pore amount. CaA zeolite exhibits the highest spatial hindered effect. Finally, co-adsorption effect of SO_2, NO, and CO_2 were investigated by multi-components breakthrough method. SO_2 and NO may form new adsorbed species, however, CO_2 presents a fast breakthrough. Chemical adsorption causes SO_2 transforms to SO_4^{2-}, however, element N and C are not detected in adsorbed zeolites.

1. Introduction

SO_2 and NO_x are the most commonly encountered air pollutants that cause acid rain and ground layer ozone formation. It is estimated that SO_2 and NO_x emission of China in 2020 will be 30.6 and 26.6 Mt, respectively [1]. On the other side, the increasing concentration of CO_2 in the air has drawn serious attention recently as it links to the global warming. It was reported that 87% of SO_2, 67% of NO_x and 71% of CO_2 emissions are from the coal combustion [2]. For the cleaning of flue gas, a few technology options are available such as wet flue gas desulfurization, NO_x selective catalytic reduction and carbon capture technology [3–5]. However, they are often multi-step, complex, and costly. It is highly desirable to have a suitable single-step process for the simultaneous removal of SO_2, NO_x, and CO_2 from the flue gas. Adsorption process may offer a promising way for the removal of SO_2, NO_x, and CO_2 in flue gas simultaneously because of the minimum energy requirements, relatively simple design and minimum waste disposal problems.

Fortunately, there are many literatures related to the purification of single pollutant by adsorption method. Adsorption removal of SO_2 in flue gas would be a promising alternate for lime-base scrubbing due to the more stringent regulations [6,7]. The NO_x storage technology also makes big progress. The most important part of this technology lies in its adsorption properties and many researches focus on that area [8,9]. Carbon capture by adsorption method draws more and more attention recently [10]. Given that all these pollutants co-exist in flue gas, adsorption method seems to remove SO_2, NO_x, and CO_2 simultaneously. However, no literature can be found as a precursor to consider removal of SO_2, NO_x, and CO_2 all together.

The correct selection of adsorbents is a very important procedure for adsorption system design. Zeolites are microporous crystalline materials with uniform-shaped pores of molecular dimensions, which are commonly used for gas separation and catalysis [11]. It was reported that zeolites are the prospective adsorbents for removal of SO_2 from industrial gas [12,6]. Selective adsorption of NO_x in flue gas by zeolite was also reported in the literature [13]. Carbon capture by zeolite adsorption has been widely considered [14,15]. The SO_2, NO_x, and CO_2 adsorption process is a new development for the simultaneous removal of SO_2, NO_x, and CO_2 in flue gas. Zeolite may show a very promising future in the cleaning of flue gas.

Taking account of that the former researches are relatively independent and often focus on adsorption of one component. Furthermore, the adsorption equilibrium and kinetic character were not studied thoroughly. So the objective of this work is several-fold. (1) The adsorption isotherms for SO_2, NO, and CO_2 were obtained on NaY, NaX, CaA zeolite, and the equilibrium character about both adsorbate and adsorbent were analyzed based on isotherm model and Henry's constant. (2) In order to assess the dynamic performance of SO_2, NO, and CO_2 on zeolites, kinetic studies were carried out by breakthrough experiment. (3) The best performance

* Corresponding author. Tel.: +86 871 5170905; fax: +86 871 5170906.
E-mail address: txl-km@163.com (X. Tang).

0304-3894/$ – see front matter
doi:10.1016/j.jhazmat.2011.11.091

Nomenclature

b	Langmuir constant
C_0	initial concentration (ppm)
d_p	particle diameter (m)
D_c	micropore diffusivity ($m^2\ s^{-1}$)
D_k	Knudsen diffusivity ($m^2\ s^{-1}$)
H	height of bed (mm)
K_H	The Henry's constant (mmol $g\ g^{-1}\ Pa^{-1}$)
k_f	external phase mass transfer coefficient ($m\ s^{-1}$)
M	molecular weight ($g\ mol^{-1}$)
n	Freundlich equation parameter
q_s	concentration adsorbed on the surface
q	moles of adsorbate adsorbed per unit mass of adsorbent (mmol g^{-1})
q_{max}	maximum adsorbed phase concentration (mmol g^{-1})
R_c	radius of microparticle (m)
Re	Reynolds number
S_p	external area ($m^2\ m^{-3}$)
u	superficial velocity ($m\ s^{-1}$)
z	axial coordinate along the bed (m)
ε_p	particle porosity
ρ_w,	wall density ($kg\ m^{-3}$)
C	gas concentration (ppm)
C_s	gas concentration at the surface
D	fluid flow (ml min^{-1})
D_e	effective diffusivity ($m^2\ s^{-1}$)
D_m	molecular diffusivity ($m^2\ s^{-1}$)
K_0	equilibrium constant
K	Freundlich equation parameter
k_p	mass transfer coefficient (s^{-1})
K_m	transfer coefficient ($cm\ s^{-1}$)
P	pressure (Pa)
R^2	correlation coefficent
R_p	particle radius (m)
r_0	mean pore radius (m)
Sc	Schmidt number
t	time (min)
T	temperature (K)
W	bed weight (kg)
ε	porosity of adsorbent bed
ρ	particle density ($kg\ m^{-3}$)
τ	tortuosity

adsorbent may be picked out based on the former equilibrium and kinetics studies. How this adsorbent can be used in the combined SO_2, NO, CO_2 removal was investigated finally.

2. Materials and methods

2.1. Materials

Zeolite samples (NaX, NaY, and CaA) used in this work were pellets (2.5–5 mm) from the catalyst plant of Nankai University, Tianjin, China. The specific surface areas and pore volume for the samples were determined by N_2 adsorption using a Micromeritics instrument. The samples were first vacuumed at 573 K for more than 12 h before adsorption isotherms were generated by dosing nitrogen (at 77 K) on the adsorbents. The textural data were summarized in Table 1.

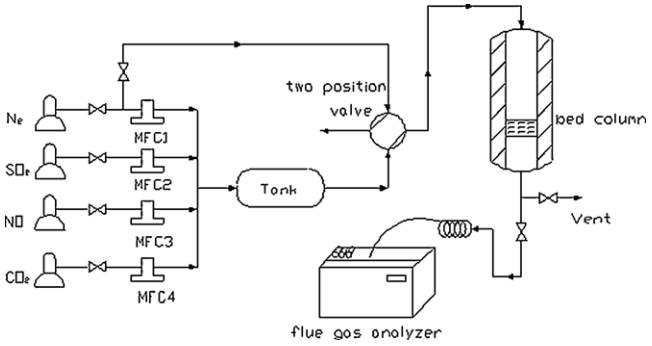

Fig. 1. Experimental setup for adsorption in a fixed-bed column (MFC, mass flow controller).

2.2. Experiments

2.2.1. Adsorption equilibrium measurements

Equilibrium isotherms of SO_2, NO, and CO_2 were measured using a static volumetric adsorption instrument. The details about the experimental set-up and operational conditions were presented elsewhere [16]. It was noteworthy that the sample was heat up to 373 K with blowing inert gas (Helium, 99.99%) to wash the instrument and clear the adsorbent in the adsorption system before every measurement. Adsorbate purities were 99.9%, 99.5%, 99.9% and 99.99% (v%) for SO_2, NO, CO_2 and N_2, respectively.

2.2.2. Column adsorption experiments

Fig. 1 shows a schematic diagram of the laboratory system used for measuring breakthrough curve. The reactor was constructed from a quartz glass tube of 18 mm i.d. and 200 mm length. The whole reactor was located inside a furnace with controlled temperature. Gauze plate of fine mesh and thin layer of glass wool were placed at both ends of the bed to hold packing in position and prevent heat loss from column ends. The velocity of inlet and outlet or reactor was measured by soap foam flowmeter with flow of N_2, no pressure decrease was found in our experiment. SO_2, NO, and CO_2 were supplied by pressurized cylinder. Concentration for SO_2, NO, CO_2 and N_2 cylinder were 1%, 1%, 99.9% and 99.99% (v%), respectively. The adsorbents NaX, NaY, CaA were crushed and sieved to 0.25–0.38 mm. Delivery of the feed gas was controlled by mass flowmeters. After mixed in a mixing tank, simulated gas was fed into the inlet of the quartz glass reactor. Prior to all measurements, an initial degassing of the sample was performed at 120 °C under the flow of nitrogen overnight. Then mixed gas was passed through the fixed bed column at constant temperature. The inlet and outlet concentration were analyzed by Kane KM9106 flue gas analyzer with additional infrared module, which has resolution for SO_2, NO, and CO_2 are 1 ppm, 1 ppm, and 0.1% respectively. Dynamic experimental conditions employed in these measurements were detailed in Table 2.

2.3. Theory and methods

2.3.1. Isotherm fitting

It is convenient to represent experimental equilibrium isotherms by analytical expressions. Many models have been proposed to describe the isotherms, for example, Langmuir, BET, and Toth. In this study, the Freundlich and Langmuir equations were used to correlate the experimental data due to their adjustable parameters and simple math expressions [17]. These equations were presented as follows:

Freundlich isotherm : $q = KP^{1/n}$ (1)

Table 1
The textural parameters of zeolites NaY, NaX, and CaA.

	Specific surface area ($m^2\ g^{-1}$)	Total pore volume ($cm^3\ g^{-1}$)	Micropore volume ($cm^3\ g^{-1}$)	Average pore diameter (nm)
NaY	542	0.38	0.19	3.29
NaX	534	0.29	0.22	2.88
CaA	397	0.32	0.15	2.27

Table 2
Experimental conditions for breakthrough curve.

T, temp (K)	323.15
P, pressure (Pa)	82,425
D, fluid flow ($ml\ min^{-1}$)	200
ε, bed porosity	0.42–0.45
H, bed height (mm)	12–55
u, superficial velocity ($m\ s^{-1}$)	0.0106
ρ, bed density ($kg\ m^{-3}$)	429–560
W, bed weight (kg)	0.0795
ρ_w, wall density ($kg\ m^{-3}$)	2184
Gas composition (balance gas: N_2)	
SO_2	2000 ppm
NO	1000 ppm
CO_2	10%

$$\text{Langmuir isotherm}: \quad q = \frac{q_m b P}{1 + bP} \tag{2}$$

A non-linear least-squares regression based on Gauss–Newton method was used to fit Freundlich and Langmuir to experimental equilibrium isotherms data. Parameters of each equation and the agreement between experimental and calculated adsorption isotherms in terms of correlations coefficients were given by MATLAB 7.0.

2.3.2. Adsorption affinity

In order to evaluate adsorption affinity between adsorbate and adsorbent, the Henry's constant was investigated. The constant was directly related to the interaction of molecules with the surface of the adsorbent since at low pressure, molecule-surface forces predominated [18]. According to the property of Virial model, Henry's constant can be determined as follows:

$$\frac{P}{q} = \frac{1}{K_H} \exp\left(2A_1 q + \frac{3}{2}A_2 q^2 + \frac{4}{3}A_3 q^3 + \cdots\right) \tag{3}$$

where A_1, A_2 and A_3 are the Virial coefficients. A plot of $\ln(P/q)$ vs the loading q, should approach the axis linearly as q close to 0 with slope $2A_1$ and intercept $-\ln(K_H)$.

2.3.3. Modeling of breakthrough curve

The mathematical model of the isothermal, dynamic adsorption breakthrough process in a fixed bed is based on transient material balance, gas phase and intrapellet mass transfer, the adsorption equilibrium relationship, boundary conditions, and initial conditions. Liner driving force model (LDF) seems to suitable choice for simulating adsorption breakthrough curve [19,20]. The assumptions made are common: (1) the pressure drop is very low, the velocity and density of the fluid are constant; (2) the system is isothermal during whole process based on experimental observation of 1 K maximum temperature swing; (3) the vapor is considered as an ideal gas; and the plug flow is assumed; (4) effect radial and axial dispersion are neglected; (5) bed porosity is uniform. The mass balance on a portion of the bed is given by

$$\varepsilon\frac{\partial C}{\partial t} + \rho\frac{\partial q}{\partial t} + u\frac{\partial C}{\partial z} = 0 \tag{4}$$

The lumped-parameter LDF model was used to describe the intrapellet mass transfer as follows:

$$\frac{\partial q}{\partial t} = k_p(q_s - q) \tag{5}$$

Equality of flux through the surface of the adsorbent leads to the following continuity equation:

$$k_f S_p(C - C_s) = \rho k_p(q_s - q) \tag{6}$$

Concentration of the compound at the column inlet is the initial concentration, C_0:

$$C = C_0 \quad \text{for} \quad z = 0 \quad \text{and} \quad t > 0$$

Initial conditions:

$$q = 0 \quad \text{for} \quad z \geq 0 \quad \text{and} \quad t = 0$$

$$C = C_0 \quad \text{for} \quad z = 0 \quad \text{and} \quad t = 0$$

$$C = 0 \quad \text{for} \quad z > 0 \quad \text{and} \quad t = 0$$

The numerical method was the Finite Difference Method. Backward finite difference explicit scheme was used in this study. The k_p parameter can be considered as an adjustable parameter. Thus, fitting simulation results and experimental data allows this parameter to be determined.

The LDF mass-transfer coefficient k_p is related to mass-transfer resistance for a adsorbent as follows [19–21]:

$$\frac{1}{k_p} = \frac{R_p}{3k_f} + \frac{R_p^2}{15\varepsilon_p D_e}K_e + \frac{R_c^2}{15D_c} \tag{7}$$

The LDF global mass transfer coefficient considers all of the resistances to the mass transfer, i.e. intra- and extra particle resistances. It considers film resistance, macropore and micropore resistances.

The k_f coefficient can be evaluated by means of film mass transfer expression [16]:

$$k_f = 1.09Re^{0.27}Sc^{0.33}\frac{D_m}{d_p} \tag{8}$$

The molecular diffusivity D_m is approximated with the Chapman–Enskog equation.

The effective diffusivity (D_e) is related to molecular, Knudsen, and surface diffusivities, which can simply be calculated by means of Bosanquet equation [19,21]:

$$\frac{1}{D_e} = \tau\left(\frac{1}{D_m} + \frac{1}{D_k}\right) \tag{9}$$

where Knudsen diffusivity is given by the relation:

$$D_k = 9700 r_0\sqrt{\frac{T}{M}} \tag{10}$$

The values of k_p, k_f and D_e can be calculated directly according to the equations (4–5, 8–10), the micropore diffusivity D_c can be deduced by Eq. (7) with the known values of k_p, k_f and D_e.

For measuring the relative resistance contributed by the film surrounding the particle to the internal diffusion resistance, Biot number was calculated as follows:

$$Bi = \frac{K_m R_p}{\varepsilon D_c} \tag{11}$$

when Biot number is greater than about 50, the mass transfer resistance in the stagnant film surrounding the particle can be neglected compared to the internal diffusion.

Table 3
Isotherm results for SO_2, NO, and CO_2 correlated with Freundlich and Langmuir model.

		SO_2			NO			CO_2		
		K	n	R^2	K	n	R^2	K	n	R^2
NaY	Fruendlich	0.000241	1.219	0.9976	0.000102	1.811	0.9724	3.7×10^{-6}	1.101	0.977
NaX		0.000999	1.34	0.9948	0.000881	2.234	0.9958	0.000293	1.312	0.988
CaA		0.01178	2.165	0.9552	0.000856	2.202	0.998	0.005256	2.017	0.9842
		SO_2			NO			CO_2		
		q_m	$b \times 10^6$	R^2	q_m	$b \times 10^6$	R^2	q_m	$b \times 10^6$	R^2
NaY	Langmuir	5.398	8.972	0.9941	0.0621	33.91	0.9508	1.454	1.007	0.9834
NaX		6.473	17.61	0.9962	0.1581	48.52	0.9788	2.918	12.22	0.996
CaA		2.125	72.58	0.9921	0.1644	47.41	0.9782	1.658	42.37	0.9987

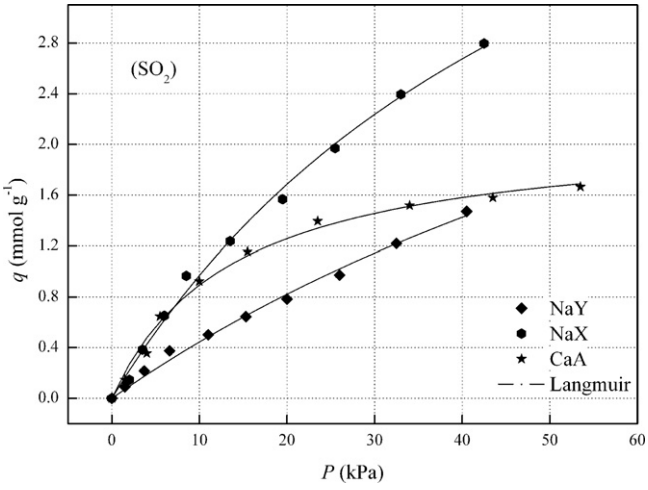

Fig. 2. Adsorption isotherms of SO_2 on zeolite NaY, NaX, and CaA at 323 K.

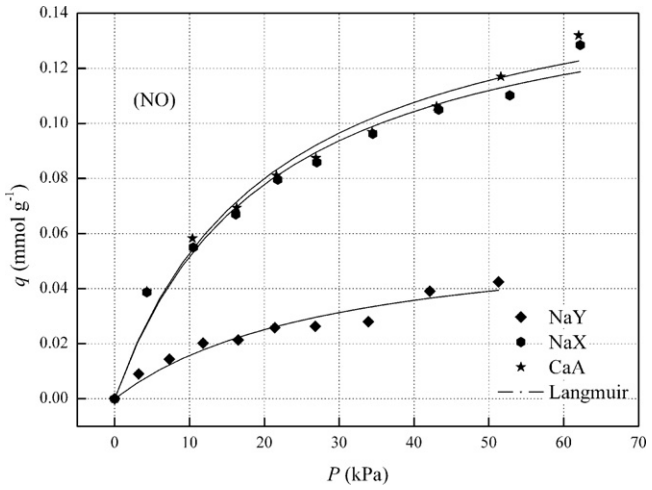

Fig. 3. Adsorption isotherms of NO on zeolite NaY, NaX, and CaA at 323 K.

3. Results and discussion

3.1. Adsorption equilibrium analysis

The adsorption isotherms of SO_2, NO and CO_2 on NaY, NaX, and CaA zeolites were obtained at 323 K, respectively. Freundlich and Langmuir were used to correlate to the experimental data. The equation parameter and agreement parameter were listed in Table 3. It can be found that Langmuir is suitable for describing the adsorption of SO_2 and CO_2 on zeolites. However, Freundlich fits better for adsorption of NO on zeolites. For the sake of convenience, all adsorption isotherms are described by Langmuir equation. As shown in Figs. 2–4, all isotherm shape can be classified as Type-I according to the IUPAC classification. It is coincident with the adsorption character of microporous materials.

The effect of adsorbate can be observed in Figs. 2–4, and the adsorption capacity follow the order $SO_2 > CO_2 > NO$. For the same adsorbate, the adsorption capacity of different adsorbents generally decrease in the sequence CaA > NaX > NaY. Exception was found for SO_2 on NaX zeolite, which exhibits higher adsorption loading than CaA zeolite when pressure increases beyond 10 kPa.

In order to understand the equilibrium differences profoundly, the Henry's law constant was calculated by Virial plot method. The results were summarized in Table 4. Since the constant is directly related to the interaction of molecules with the surface of the adsorbent. The higher is value of the constant, the stronger affinity exhibit between adsorbate–adsorbent pair. As shown in the Table 4, the Henry's constant value decrease in the trend $SO_2 > CO_2 > NO$ on the all adsorbents except for NaY. The effect may attribute to the adsorbate molecular multiple moment and polarizability. SO_2 has the highest permanent dipole moment and polarizability, which cause

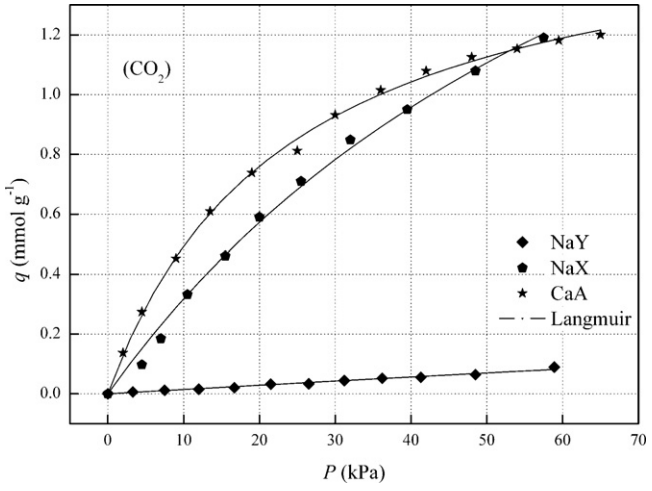

Fig. 4. Adsorption isotherms of CO_2 on zeolite NaY, NaX, and CaA at 323 K.

it has strongest electrostatic and dispersion interaction with the same adsorbent. Even though CO_2 does not possess dipole moment, the highest quadrupole moment and the second highest polarizability make the affinity between the same adsorbent stronger than that of NO. However, stronger affinity was found in adsorption of NO on NaY zeolite than CO_2. This difference may originate from the surface polar properties of NaY zeolite. Because of the highest Si/Al ratio, NaY exhibits the most non-polarity and the induce interaction with CO_2 turns week. For the same adsorbate, the adsorbent effect follow the order CaA > NaX > NaY according to the Table 4. It can be

Table 4
Henry's constants for SO_2, NO, and CO_2 on different zeolites.

K_H ($\times 10^6$)	SO_2	NO	CO_2
NaY	48.4	2.13	1.46
NaX	114	8.09	35.8
CaA	168	8.19	73.1

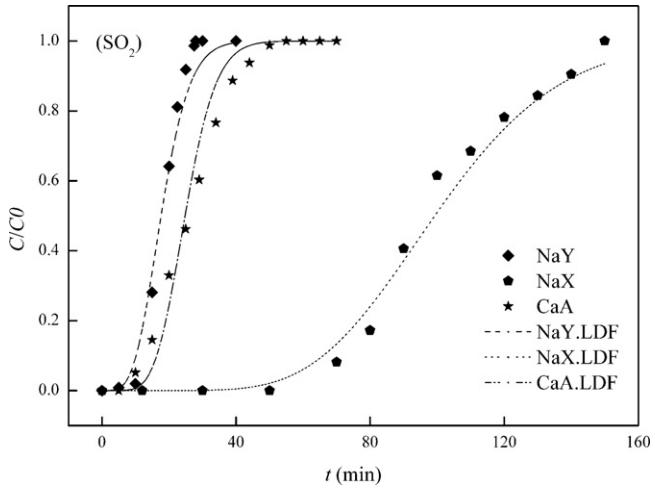

Fig. 5. Experimental and predicted breakthrough curves of SO_2 on zeolites (SO_2, 2000 ppm; N_2, balance gas; adsorbents, 2 g).

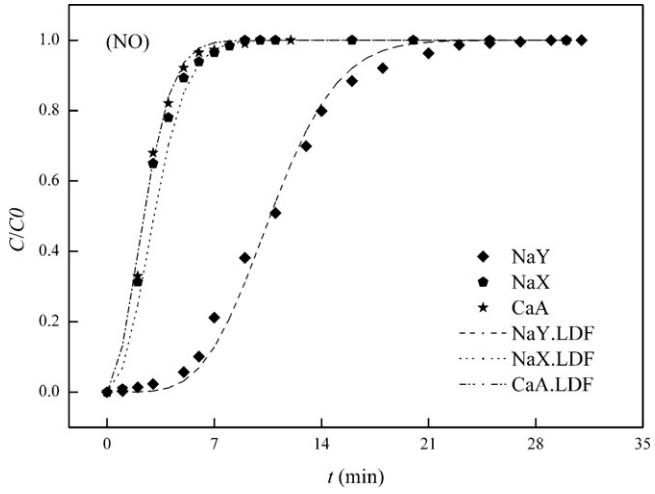

Fig. 6. Experimental and predicted breakthrough curves of NO on zeolites (NO, 1000 ppm; N_2, balance gas; adsorbents, 6 g).

explained by the polar nature of zeolites. Zeolite CaA has the most negative charge and bivalent cation Ca^{2+} balances the gap, which makes the surface exhibits highest polarity. NaX and NaY have the same structure and the same cation Na^+ dispersed, however, NaX zeolite presents higher polar feature due to its lower Si/Al ratio. It can be deduced that zeolites with stronger polarity properties are more promising in improvement of adsorption capacity.

3.2. Kinetics study

The breakthrough simulations of SO_2, NO and CO_2 on different zeolites were performed using the LDF model described in Section 2 at 323 K respectively. The experimental data and simulated curves are presented in Figs. 5–7. It can be found that the linear driving force model is suitable for description of SO_2, NO and CO_2 on NaY, NaX and CaA zeolites in a fixed-bed column. The overall

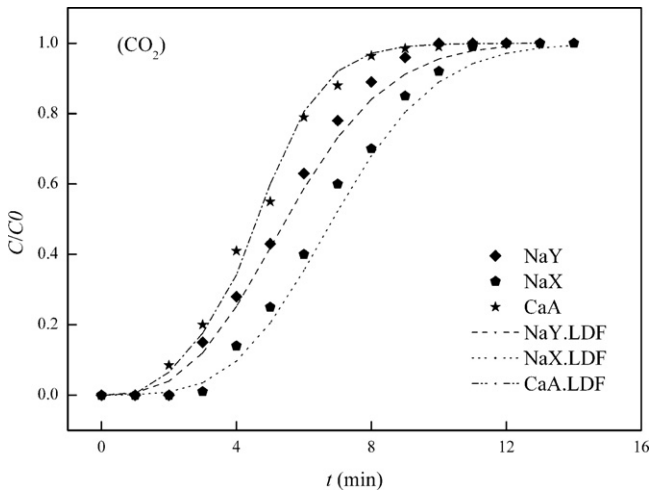

Fig. 7. Experimental and predicted breakthrough curves of CO_2 on zeolites (CO_2, 10% (v); N_2, balance gas; adsorbents, 6 g).

Table 5
Summary of mass transfer parameters derived from breakthrough curve and diffusivity parameters.

	NaY	NaX	CaA
SO_2			
k_p	0.103	0.069	0.051
k_f	7.72	7.8	7.73
D_e	0.00043	0.0004	0.00027
D_c/r_c^2	0.0069	0.0047	0.0034
Bi	1075	1057	1080
NO			
k_p	0.612	0.0702	0.084
k_f	14.9	14.98	14.91
D_e	0.00044	0.0004	0.00027
D_c/r_c^2	0.0408	0.0047	0.0056
Bi	4500	4480	4500
CO_2			
k_p	0.481	0.035	0.026
k_f	8.79	8.86	8.8
D_e	0.00063	0.00058	0.00039
D_c/r_c^2	0.0321	0.0023	0.0017
Bi	4495	4565	4588

mass transfer parameters used for the simulation and diffusivity factors calculated by Eqs. (7)–(11) are listed in Table 5. To estimate the pore diffusivity coefficient, a tortuosity factor of 4 and a pellet porosity of 0.5 were assumed for zeolites [19].

According to the experimental results where the Bi number far higher than that of 50, it suggest that film resistances show limited effect on the global mass transfer resistances, thus the intraparticle diffusion in the pores is predominant and the external mass transfer resistance can be neglected for all gases studied. Compared with the micropore resistance where the magnitude of crystal radius is at least 10^{-6} m, the macropore resistances effect is either not significant duo to its small quantity. Thus the overall mass transfer resistance derived from the micropores.

Our observation of global mass transfer coefficient k_p value are in close agreement with other literature [20,22]. As it follows from the table, k_p value for the same adsorbate increases in the following trend CaA < NaX < NaY. Such an order can be explained through the pore distribution as shown in Fig. 8. Zeolite NaY has the most efficient mass transfer because of its widest pore distribution and highest pore volume. Even through zeolites NaX and CaA have similar pore distribution, the least pore amount of CaA prohibits the mass transfer process. The highest diffusion rate makes the mass transfer zone in adsorbent bed narrow. So NaY zeolite will be saturated to a great extent than other zeolite in spite of NaY

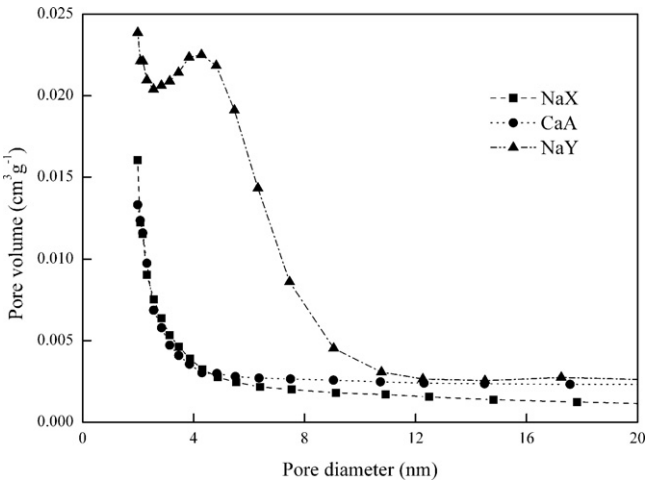

Fig. 8. Pore distribution of zeolites NaY, NaX, and CaA.

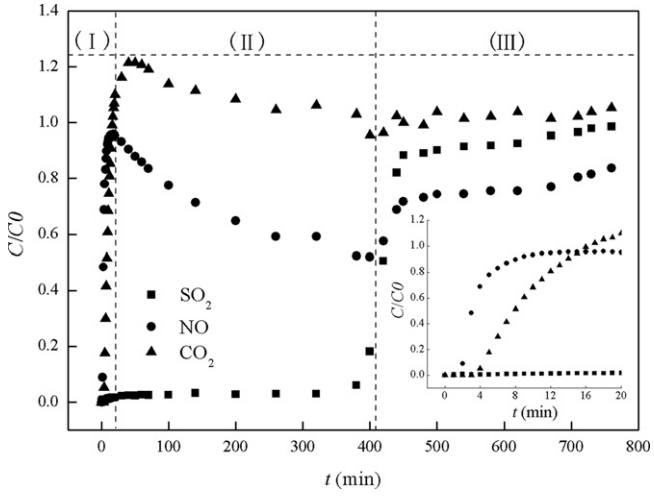

Fig. 9. Breakthrough curves of SO_2, NO, and CO_2 co-adsorption on NaX zeolite (2000 ppm SO_2, 1000 ppm NO, 10% CO_2, balance gas: N_2, NaX zeolite: 6 g).

zeolite has the lowest equilibrium adsorption capacity. For different adsorbates, the serial increases like $CO_2 < SO_2 < NO$ with the same adsorbent. Considering that kinetic diameters for SO_2, NO, and CO_2 are 0.36, 0.32, and 0.33 nm, respectively [23,24]. The average pore opening for NaY, NaX, and CaA zeolites are 3.29, 2.88, and 2.27 nm as shown in Table 1. No spatial hindering effect was found in the adsorption process. It suggests that NO with the fastest diffusion speed moves quickly than other components and can be adsorbed in the fresh zeolites downstream of the bed.

3.3. Co-adsorption breakthrough curve

According to the analysis before, zeolite NaX has the eclectic results on equilibrium capacity and kinetics resistance. It could be a good candidate for co-adsorbing SO_2, NO, and CO_2 in flue gas. Thus the co-adsorption breakthrough experiment was performed under mixture gas. The experiment condition and results were presented in Fig. 9.

It can be observed that the shape of the SO_2 breakthrough curve is not modified much. However, the breakthrough curve for NO and CO_2 show an interesting behavior. The shape of NO breakthrough curve sharply ascends at first. After the initial breakthrough, the NO concentration descends to a minimum and then gradually ascends. Similar behavior was found for the shape of CO_2 breakthrough curve. The difference between CO_2 and NO is that a level off trend for CO_2 appeared after an outlet concentration decrease.

Three phases can be defined for all breakthrough curves. The approximately demarcation were plotted in Fig. 9. (1) Breakthrough phase, where NO and CO_2 quickly breakthrough the fixed-bed while almost SO_2 are trapped in the bed. NO exhibits the fast breakthrough speed, which may attribute to the sum of the minimum equilibrium adsorption capacity and the fastest diffusivity. (2) Competition phase, where SO_2 still diffuses in the upstream of the bed while NO and CO_2 show a decrease trend in concentration. It is noticeable that the outlet concentration of CO_2 is higher than that of inlet. It indicates that the adsorbed CO_2 is replaced by other components. The value of C/C_0 for NO in this phase monotonously descends and is less than unity. It suggests that adsorption amount of NO is scarcely affected by the replacement of SO_2. Adsorbed NO and SO_2 may create new intermediate species [25] and finally increase in adsorption capacity of NO is found. (3) Saturation phase, when SO_2 begins to breakthrough, NO is no longer to decrease but to breakthrough again. Both components present a trend to saturation. During this process, some CO_2 still be substituted. It implies that CO_2 is on an inferior position in the adsorption system.

In order to understand the adsorption mechanism thoroughly, XPS characterization of zeolite NaX before and after co-adsorption were completed and the results were summarized in Table 6. It can be observed from the table that all binding energy of Al, Si, and Na element in NaX zeolite are consistent with the X type zeolite. After co-adsorption, element S was definitely found on the surface of NaX zeolite with the chemical state of SO_4^{2-}. However, element N and C were not detected in our experiment. For proofing this finding, we also simulated co-adsorption system by equilibrium species calculation using Factsage 6. Consistent results were found between the experiment and simulation about the chemical adsorption of SO_2. Molecule CO_2 kept the original chemical state during the co-adsorption. It seems that CO_2 has been physical adsorbed. However, NO exhibits a possible path to form harmless N_2 according to the equilibrium calculation.

Table 6
XPS results of sample NaX zeolite before and after co-adsorption of SO_2, NO, and CO_2.

Nature form (ev)	NaX (before test)	NaX (after test)
Al (2p) (72.95, 72.55)	74.76	74.78
Si (2p) (99.82, 99.42)	(103.17, 101.40)	(103.16, 101.38)
Na (1s) (1070.8)	1072.26	1072.16
O (1s) (543.1)	(533.00, 531.73)	(533.01, 531.72)
S (2p) (163.6, 162.5)	–	169.73

4. Conclusions

In order to develop a single-step process for removing SO_2, NO, and CO_2 in flue gas simultaneously. Two angle of view about pure component equilibrium and kinetics data of SO_2, NO, and CO_2 on zeolites NaY, NaX, CaA were analyzed. Equilibrium data exhibited that adsorption affinity follow the trend $SO_2 > CO_2 > NO$ on the same adsorbent. Zeolite with stronger polar surface was a promising adsorbent candidate. Kinetics behavior suggested that all adsorptions are controlled by micropore diffusion. NaY zeolite had the minimal mass transfer resistance duo to its wide pore distribution and large pore amount. Finally, co-adsorption of SO_2, NO, and CO_2 on NaX zeolite was carried out based on its compatible equilibrium and kinetics advantages. NO exhibited an interesting increase in

adsorption amount. That may attribute to the formed intermediate species with SO_2. However, CO_2 presented a fast breakthrough. Chemical adsorption causes SO_2 transforms to SO_4^{2-}, however, element N and C are not detected in adsorbed zeolites.

Acknowledgements

The work was supported by the National Natural Science Foundation of China(21077047) and Young, Middle-aged Academic and Technical Back-up Personnel Program of Yunnan Province (2007PY01-10).

References

[1] D.G. Streets, S.T. Waldhoff, Atmos. Environ. 34 (2000) 363–374.
[2] X.C. Xu, C.H. Chen, H.Y. Qi, R. He, C.F. You, G.M. Xiang, Development of coal combustion pollution control for SO_2 and NO_x in China, Fuel Process. Technol. 62 (2000) 153–160.
[3] R.K. Srivastava, W. Jozewicz, Flue gas desulfurization: the state of the art, J. Air Waste Manage. Assoc. 12 (2001) 1676–1688.
[4] G. Busca, L. Lietti, G. Ramis, Chemical and mechanistic aspects of the selective catalytic of NO_x by ammonia over oxide catalysts: A review, Appl. Catal. B: Environ. 18 (1998) 1–36.
[5] A.B. Rao, E.S. Rubin, A technical, economic, and environmental assessment of amine-based CO_2 capture technology for power plant greenhouse gas control, Environ. Sci. Technol. 36 (2002) 4467–4475.
[6] A. Srinivasan, M.W. Grutzeck, The adsorption of SO_2 by zeolites synthesized from fly ash, Environ. Sci. Technol. 33 (1999) 1464–1469.
[7] E. Ivanova, B. Koumanova, Adsorption of sulfur dioxide on natural clinoptilolite chemically modified with salt solutions, J. Hazard. Mater. 167 (2009) 306–312.
[8] W. Klose, S. Rincon, Adsorption and reaction of NO on activated carbon in the presence of oxygen and water vapour, Fuel 86 (2007) 203–209.
[9] J. Yang, T.T. Zhuang, F. Wei, et al., Adsorption of nitrogen oxides by the moisture-saturated zeolites in gas steam, J. Hazard. Mater. 162 (2009) 866–873.
[10] S. Sjostrom, H. Kruka, Evaluation of solid sorbents as a retrofit technology for CO_2 capture, Fuel 89 (2010) 1298–1306.
[11] Y. Liu, T.M. Bisson, H.Q. Yang, Z.H. Xu, Recent developments in novel sorbents for flue gas clean up, Fuel Process. Technol. 91 (2010) 1175–1197.
[12] A. Gupta, V. Gaur, N. Verma, Breakthrough analysis for adsorption of sulfur-dioxide over zeolites, Chem. Eng. Process. 43 (2004) 9–22.
[13] N. Xing, X.P. Wang, Q. Yu, X.W. Guo, Adsorption performance of zeolites for NO and NO_2, Chin. J. Catal. 28 (2007) 205–209.
[14] P.J.E. Harlick, F.H. Tezel, An experimental adsorbent screening study for CO_2 removal from N_2, Micropor. Mesopor. Mater. 76 (2004) 71–79.
[15] Z. Yong, V. Mata, A.E. Rodrigues, Adsorption of carbon dioxide at high temperature: a review, Sep. Purif. Technol. 26 (2002) 195–205.
[16] Q.F. Yu, X.L. Tang, H.H. Yi, P. Ning, L.P. Yang, L.N. Yang, L.L. Yu, H. Li, Equilibrium and heat of adsorption of phosphine on $CaCl_2$-modified molecular sieve, Asia Pac. J. Chem. Eng. 4 (2009) 612–617.
[17] D.D. Do, Adsorption Analysis, Imerial College Press, London, 1998.
[18] F.N. Ridha, P.A. Webley, Anomalous Henry's law behavior of nitrogen and carbon dioxide adsorption on alkali-exchanged chabazite zeolites, Sep. Purif. Technol. 67 (2009) 336–343.
[19] B. Stephan, H.M. Marie, N.F. Jean, Mass transfer in VOC adsorption on zeolite: experimental and theoretical breakthrough curves, Environ. Sci. Technol. 35 (2001) 3571–3575.
[20] B.C. Pan, F.W. Meng, X.Q. Chen, Application of an effective method in predicting breakthrough curves of fixed-bed adsorption onto resin adsorbent, J. Hazard. Mater. B124 (2005) 74–80.
[21] T.L.P. Dantas, S.M. Amorim, F.M.T. Luna, Adsorption of carbon dioxide onto activated carbon and nitrogen-enriched activated carbon: surface changes, equilibrium, and modeling of fixed-bed adsorption, Sep. Sci. Technol. 45 (2010) 73–84.
[22] A. Claudino, J.L. Sores, R.F.P.M. Moreira, Adsorption equilibrium and breakthrough analysis for NO adsorption on activated carbons at low temperatures, Carbon 42 (2004) 1483–1490.
[23] D.R. Lide, CRC Handbook of Chemistry and Physics, 85th edn., CRC Press, Inc., Boca Raton, 2004, pp. 193–202.
[24] L.B. Loeb, The Kinetic Theory of Gases, Dover Publications, Inc., New York, 1961.
[25] Q. Tang, Z.G. Zhang, W.P. Zhu, SO_2 and NO selective adsorption properties of coal-based activated carbons, Fuel 84 (2005) 461–465.